

## MCM-41 for Meloxicam Dissolution Improvement: *in vitro* Release and *in vivo* Bioavailability Studies

Asaad F. Hassan,<sup>\*,a</sup> Sally A. Helmy<sup>b,c</sup> and Ahmed Donia<sup>d</sup>

<sup>a</sup>Department of Chemistry, Faculty of Science, Damanhour University, 22511 Damanhour, Egypt

<sup>b</sup>Department of Pharmaceutics, Faculty of Pharmacy, Damanhour University, 22511 Damanhour, Egypt

<sup>c</sup>Department of Clinical and Hospital Pharmacy, Faculty of Pharmacy, Taibah University, 41321 AL-Madinah, AL-Munawarah, Kingdom of Saudi Arabia

<sup>d</sup>Department of Pharmaceutical Technology, Faculty of Pharmacy, Tanta University, 31511 Tanta, Egypt

In this study, MCM-41 was prepared as a carrier for poorly water soluble drugs. Meloxicam (MLX) was selected as model compound. Textural and chemical characterizations were carried out by thermal gravimetric analysis (TGA), scanning electron microscope (SEM), nitrogen adsorption/desorption, X-ray diffraction (XRD) and Fourier transform infrared (FTIR). The *in vitro* release of MLX was performed at pH 1.2 and 6.8. After loading MLX into MCM-41, its oral bioavailability was compared with the free drug and the marketed product Mobic® (R) in rabbits. After administration of free MLX to rabbits (5 mg kg<sup>-1</sup>), MLX presented a two distinct double-peak profile in case of R and F2 due to enterohepatic cycling. The effect of MCM-41 was mainly on the rate not the extent of MLX absorption. Administration of free MLX to rabbits resulted in an AUC<sub>0-∞</sub> value of 11.9 μg h mL<sup>-1</sup> and a T<sub>max</sub> of 4.3 h. When the same dose of MLX was introduced as R or formulated into MCM-41 (F2; MLX to MCM-41 ratio of 0.7), the systemic exposure to MLX was raised significantly by ca. 4-fold as reflected in AUC<sub>0-∞</sub> value of 46.9 and 45.5 μg h mL<sup>-1</sup> for R and F2, respectively. Development of an immediate formulation could enhance the curative effect of MLX by increasing its drug release and dissolution rate in the preferential absorptive region.

**Keywords:** meloxicam, MCM-41, characterization, *in vitro* release

### Introduction

Oral delivery is the preferred route for drug administration, however it is frequently impaired by several challenges such as inadequate physicochemical, biopharmaceutical and/or physiological properties that may limit their bioavailability.<sup>1,2</sup> In accordance to the biopharmaceutics classification system (BCS),<sup>3</sup> class II drugs (low solubility and high gastrointestinal (GI) permeability) present a major challenge for drug delivery system development and, in particular, in the design of suitable oral solid dosage forms. One attractive approach to increase the aqueous solubility and thus the bioavailability of poorly soluble drugs is to formulate them in their amorphous state since amorphous compounds generally exhibit higher apparent solubilities than their crystalline counterparts.<sup>4</sup>

Mesoporous silica of high surface area, large pore volume and controlled pore size distribution has attracted a great deal of attention since it was first reported by researchers at Mobil oil in 1992.<sup>5</sup> Mesoporous silica has found a wide range of applications, particularly separation,<sup>6</sup> and catalytic reactions.<sup>7</sup> Ordered mesoporous silica materials have been proposed in literature as possible carriers to improve dissolution rate of poorly soluble drugs.<sup>8-13</sup> So far, the most extensively investigated mesoporous silica as drug carrier has been the channel-like mesoporous MCM-41. MCM-41 has a hexagonal array that typically featuring a very uniform pore structure of unidirectional channels.<sup>14</sup> Furthermore, the presence of free hydroxyl groups on its surface, which is easily accessible to interactions with molecules via hydrogen bonding promote its uses in drug formulation.<sup>15</sup> Dissolution rate enhancement of class II drugs could be achieved by loading into MCM-41 due to:<sup>16</sup> (i) its high surface area allows a wide contact between solid

\*e-mail: aszm68@yahoo.com

particles and biological fluids, (ii) the unidirectional and size uniform pores shun any tortuosity and narrowing that could slow the diffusion of the adsorbed drug, (iii) the weak bonds between silicate silanols and the adsorbed molecules break easily in presence of water with consequent rapid guest release in molecular form, (iv) once adsorbed, the drug molecules are confined in a nanosized space that prevents their re-crystallization.<sup>17</sup>

Meloxicam (MLX) is an oxicam derivative and a preferential COX-2 inhibitor (Figure 1). It possesses analgesic, antipyretic and anti-inflammatory effects with less gastric and local tissue irritation as compared to other non-steroidal anti-inflammatory drugs (NSAIDs).<sup>18</sup> MLX has been found to be effective in the treatment of rheumatoid arthritis, osteoarthritis and degenerative joint diseases.<sup>19</sup> MLX is a pastel yellow solid drug belonging to BCS class II.<sup>20</sup> The solubility and dissolution rate of MLX in acid media are very poor. It is practically insoluble in water (0.012 mg mL<sup>-1</sup>),<sup>21</sup> with higher solubility observed in strong acids and bases. It is very slightly soluble in methanol. MLX has pKa values of 1.1 and 4.2. It is, therefore, considered a class II drug.<sup>20</sup> MLX is almost completely absorbed after administration with an absolute bioavailability of 89%.<sup>22,23</sup> After oral administration, it is completely absorbed over a prolonged period of time. It binds strongly to serum albumin (> 99%) and reaches a maximum concentration in 4-5 h after oral administration.<sup>24</sup> MLX is eliminated by metabolism to inactive metabolites as well as excreted unchanged in urine and feces with an elimination half-life around 20 h.<sup>22</sup>

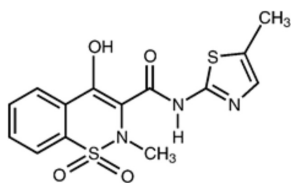


Figure 1. MLX chemical structure.

The therapeutic efficacy of MLX is strongly limited by its poor water solubility. Accordingly, a formulation which permits a fast MLX release in its absorption window could be very useful. In order to achieve this, mesoporous MCM-41 was chosen as a carrier to improve MLX dissolution rate in gastric conditions. Mesoporous silica showed potential to boost the *in vitro* and *in vivo* dissolution of poorly water soluble drugs. Several studies had been conducted for the utilization of mesoporous silica matrix MCM-41 in enhancing the dissolution of water insoluble drugs such as furosemide,<sup>16</sup> ibuprofen,<sup>25,26</sup> coumarin derivatives,<sup>27</sup> carvedilol,<sup>28</sup>

naproxen,<sup>29</sup> piroxicam.<sup>8</sup> To the best of our knowledge, very limited study had been yet reported for the dissolution enhancement of MLX by inclusion in mesoporous silica MCM-41. Accordingly, the aim of this work was to include MLX into MCM-41 pores to develop a delivery system capable to improve MLX dissolution rate in the preferential absorptive region. This was to enhance its curative and therapeutic effect.

## Experimental

### Materials

Meloxicam (purity 99%) and piroxicam (purity 99%) were purchased from Sigma-Aldrich Co., St. Louis, MO, USA. Cetyltrimethylammonium bromide (CTAB) and tetraethoxysilane (TEOS) were purchased from Alfa Aesar Co., Karlsruhe, Germany and were used without further purification. All reagents used were of liquid chromatography grade and were purchased from Merck Chemicals, Darmstadt, Germany; Milli-Q grade (Millipore, Bedford, MA, USA) distilled water was used in all cases.

### Synthesis of mesoporous MCM-41

Pure mesoporous silica MCM-41 was synthesized according to the method proposed by Beck *et al.*<sup>30</sup> CTAB, as a template, was dissolved in amount of distilled water in presence of ammonia solution. Addition of ammonia resulted in a sufficiently basic solution (ca. pH 13) to initiate the formation of silicate anions. Once fully dissolved, the silica source, TEOS, was added drop wise to the mixture with vigorous stirring at 25 °C. At higher tetraethoxysilane loading, a thick white paste was formed. The product was filtered, washed with distilled water and dried in air at 110 °C. The mole composition of the gel mixture was TEOS:CTAB:NH<sub>3</sub>:H<sub>2</sub>O = 1.04:0.22:1.39:44.4. The sample was calcined in muffle at 550 °C for 5 h.

### MLX loading in MCM-41 procedures

Three formulations of MCM-41-MLX (F1, F2 and F3) were prepared by solvent evaporation method. Three equal amounts of MCM-41 were added to a three different MLX concentrated solutions in 50 mL ethanol with MLX to MCM-41 ratios of 0.1, 0.7 and 1.4 to afford final products; F1, F2, and F3, respectively. The mixtures were kept under magnetic stirring for 48 h at room temperature. Solvent removal was performed by a rotary evaporator. The three formulations were filtered and dried in vacuum conditions at 40 °C for five days.

### Preparation of physical mixture by trituration method

MLX and MCM-41 at a ratio of 7:10 were sifted through a 40-mesh (425  $\mu\text{m}$ ) screen, mixed together (with trituration in a pestle-mortar), and stored in a desiccated environment.

### Textural and chemical characterization

Thermogravimetric analysis (TGA) for MCM-41 and MCM-41 loaded with MLX (F2) was performed in thermoanalyzer apparatus (Shimadzu D-50, Japan) at a nitrogen flow rate of 50 mL  $\text{min}^{-1}$  and a heating rate of 10  $^{\circ}\text{C min}^{-1}$  up to 850  $^{\circ}\text{C}$ .

The crystalline characteristics of MCM-41, physical mixture, and MCM-41 loaded with MLX (F2) were determined using powder X-ray diffractometer (XRD) (Shimadzu XD-1, Japan). About 60 mg of sample was run as a smear amount on a standard glass slide and a diffractogram in the  $2\theta$  range 0.5-10 with a scanning rate 2 degree  $\text{min}^{-1}$  was obtained.

Scanning electron micrographs (SEM) for MCM-41, and MCM-41 loaded meloxicam (F2) were obtained using JEOL 6400, Japan. Prior to the measurement, the sample was dried at 110  $^{\circ}\text{C}$  for 4 h. A thin layer of the gold was coated on the sample for charge dissipation.

Specific surface area ( $S_{\text{BET}}$  /  $\text{m}^2 \text{g}^{-1}$ ), total pore volume ( $V_T$  /  $\text{mL g}^{-1}$ ), and pore radius ( $\bar{r}$  /  $\text{nm}$ ) for MCM-41 and F2 samples were determined through nitrogen adsorption at  $-196$   $^{\circ}\text{C}$  using NOVA2000 gas sorption analyzer (Quantachrome Corporation, USA) system. The specific surface area ( $S_{\text{BET}}$  /  $\text{m}^2 \text{g}^{-1}$ ) was measured using BET equation. Average pore radius ( $\bar{r}$  /  $\text{nm}$ ) was calculated using the following equation:

$$\bar{r} (\text{nm}) = \frac{2V_T (\text{mL} / \text{g})}{S_{\text{BET}} (\text{m}^2 / \text{g})} \times 10^3 \quad (1)$$

where,  $V_T$  is the adsorbed volume near saturation, i.e., at  $p/p^{\circ}$  ca. 0.95 multiplied by the factor  $15.5 \times 10^{-4}$ .

Fourier transform infrared spectra (FTIR) of MCM-41, MLX, physical mixture and MCM-41 loaded with MLX (F2) were recorded on a Mattson 5000 FTIR spectrometer in the range between 4000 and 400  $\text{cm}^{-1}$ , were prepared by conventional KBr pellet method.

### *In vitro* release studies

MLX *in vitro* release was performed at pH 1.2 and 6.8 to simulate the gastric and intestinal fluids using USP-2 (paddle) dissolution apparatus (Copley Scientific, Nottingham, UK), 50 rpm and  $37 \pm 0.5$   $^{\circ}\text{C}$ . To operate in sink

conditions, each sample contained 15 mg of MLX. Five mL samples of the dissolution medium were withdrawn at appropriate time intervals (1, 2, 3, 4, 5, 10, 15, 30, 45, 60, 90 and 120 min). The samples were filtered through a 0.45  $\mu\text{m}$  Millipore filter (Merck KGaA, Darmstadt, Germany) and fresh dissolution medium preheated at 37  $^{\circ}\text{C}$  was added to compensate for the withdrawn volume. MLX content was determined spectrophotometrically (Thermo Scientific™ Evolution 300 UV-Vis Spectrophotometer, Madison WI 53711-4495 U.S.A.) at 360 nm in the two dissolution media with reference to a standard curve constructed for each dissolution medium. Each result represented an average of three measurements and the error was expressed as standard deviation (SD). The cumulative amount and percentage of drug release at each sampling time was computed, and release profiles were plotted as the cumulative percent of drug released *versus* time.

For drug release kinetics, to calculate the possible mechanism of MLX release from the tested formulations, the release data was analyzed mathematically according to the following models: Zero-order kinetic ( $Q = kt$ ) by plotting the undissolved drug amount *versus* the time,<sup>31</sup> first-order kinetics ( $\log Q = kt/2.303$ ) by plotting the logarithm of the undissolved drug amount *versus* the time,<sup>31-33</sup> and Higuchi's kinetics ( $Q = kt^{0.5}$ ) by plotting the undissolved drug amount *versus* the square root of time,<sup>34</sup> where (Q) is the amount of drug released at a time (t) and (k) is the rate constant.

The kinetic parameters of the dissolution were calculated by using equations of a mathematical model that presented most significant correlation coefficient. The calculated *in vitro* differential and cumulative release parameters were peak height (PH, % released), peak time (PT, min), and area under differential dissolution curve (AUDC, min%) for differential and area under cumulative dissolution curve (AUCC, min%) and half-life of release ( $t_{50\%}$ , min) for cumulative release parameters.

### Stability studies

MCM-41 loaded with MLX (F2) were kept at  $40 \pm 0.5$   $^{\circ}\text{C}$  and at 75% of relative humidity.<sup>15</sup> The presence of the crystalline form was tested by XRD after 1, 7, 15, 30 and 60 days. Moreover, the physical stability was evaluated by keeping the samples in a desiccator over  $\text{CaCl}_2$  for 60 days at room temperature

### *In vivo* study

#### Animal experiments

Six male New Zealand white rabbits (4-6 months of age, 2.5-3.0 kg, male) were housed according to

the Egyptian laws, guidelines and policies for animal experiments, housing and care. The animal study adhered to the principles of Institutional Animal Care and Use Committee Guidebook.<sup>35</sup> The study protocol was approved by the Institutional ethical committee for the use of animals in research. Prior to oral drug administration, the rabbits were fasted overnight (> 12 h) with free access to water. On study days, rabbits were placed in metal restrainers at 8.00 am, and a 22 gauge × 12-in catheter (Charter Med Inc., Winston-Salem, NC) was inserted without anesthesia into the anterior vena cava *via* the marginal ear vein. Doses were administered orally by gavage at 9.00 am as a 16-mL bolus of the respective formulation. After receiving the oral dose, 3 mL of water was administered to facilitate swallowing. After 4 h, the rabbits had free access to food and water.

MCM-41 loaded with MLX (F2), free MLX and Mobic® (Boehringer Ingelheim International GmbH Ingelheim am Rhein, Germany) were selected for *in vivo* study. Each animal received the three formulations as a single oral dose of 5 mg kg<sup>-1</sup> in a complete three cross-over design with a 2-week washout period. Blood samples (1 mL) were collected through the marginal ear vein catheter by insulin plastic syringe at 0.5, 1, 2, 3, 4, 5, 6, 7, 8, 10, 12 and 24 h after drug administration. Immediately after blood collection, plasma was harvested by centrifugation at 3000 g for 10 min. Plasma was then transferred to a fresh Eppendorf tube and frozen at -20 °C prior to analysis by a validated high performance liquid chromatography (HPLC) method. After collection of the final blood samples at 24 h after dosing, catheters were removed and the rabbits were returned to their cages.

#### HPLC assay

The plasma level of MLX was measured using a validated HPLC-UV method.<sup>24</sup> Briefly, the mobile phase comprised 0.6% acetic acid: acetonitrile, at a ratio of 52:48; the elution was isocratic at ambient temperature with a flow rate of 2 mL min<sup>-1</sup>. The separation was achieved using a  $\mu$  Bondapak<sup>TM</sup> C<sub>18</sub> column (300 mm × 3.9 mm, 15-20  $\mu$ m; Waters, U.S.A.). The effluent was monitored using a Waters 2487 dual  $\lambda$  absorbance detector, U.S.A. at 364 nm for MLX and the internal standard (piroxicam), and peak areas were integrated and calculated electronically using the data analysis program Millenium. The calibration curves included all drug concentrations measured in clinical practice with within- and between-day accuracies and precisions were in accordance with Food and Drug Administration (FDA) guidelines.<sup>36</sup> Calibration curves (n = 7) were found to be linear over the entire concentration range of MLX (0.05-10  $\mu$ g mL<sup>-1</sup>), with a correlation coefficient  $R^2 > 0.999$  throughout the course of the assay for

MLX. The lower limit of quantification (LOQ) and limit of detection (LOD) were 0.05 and 0.02  $\mu$ g mL<sup>-1</sup>, respectively. The within- and between-day coefficients of variance (CV) were always within  $\pm 12\%$  in the entire range of the calibration curve. The within-day accuracy ranged between 99.9% and 107.0%, whereas the between-day accuracy ranged between 98.7% and 103.1%. The concentrations of the quality control samples were 0.1, 5 and 7  $\mu$ g mL<sup>-1</sup>, respectively. The absence of interference of MLX with piroxicam was verified.

#### Pharmacokinetic analysis

Individual plasma concentration-time profiles were analyzed according to non-compartmental pharmacokinetic (PK) analysis. The elimination rate constant (k) was estimated by least squares regression of plasma concentration-time data points in the terminal log-linear region of the curves. Half-life ( $t_{1/2}$ ) was calculated as 0.693 divided by k. The AUC from zero to the last measurable plasma concentration ( $AUC_{0-t}$ ) was calculated using the linear trapezoidal rule. The AUC from zero to infinity ( $AUC_{0-\infty}$ ) was calculated as  $AUC_{0-t} + C/k$ , where C is the last measured concentration.<sup>36</sup> The non-compartmental parameters describing the concentration and location of the two peaks ( $C_{max 1}$ ,  $C_{max 2}$  and  $T_{max 1}$ ,  $T_{max 2}$ ). The Apparent total clearance (Cl/F) was calculated as oral clearance ( $Cl/F$ ) = dose/ $AUC_{0-\infty}$ . The apparent volume of distribution ( $V_d/F$ ) was estimated as oral clearance/k relative to the bioavailability (F) of MLX. Area under the first moment curve (AUMC) was calculated by trapezoidal integration and extrapolation to infinity. Mean residence time (MRT) was calculated as the ratio ( $AUMC/AUC_{0-\infty}$ ).<sup>37</sup>

#### Statistical analysis

The PK parameters were calculated and the results presented as the mean  $\pm$  SD. Statistical comparisons between phases were made with Student's *t*-test and one-way analysis of variance (ANOVA). All statistical analyses were performed using the Minitab Statistical Package version 13 (Minitab, State College, PA) on an IBM PC. A *p* value of  $\leq 0.05$  was taken as the level of significance.

## Results and Discussion

#### Textural and chemical characterization

Surface and structural properties of nanoporous solids could be studied directly by employing modern techniques such as electron microscopy, atomic force microscopy, X-ray analysis and various spectroscopic methods suitable for materials characterization and surface imaging.<sup>38</sup> In

addition, these properties could be investigated by indirect methods such as adsorption,<sup>39</sup> and thermal analysis.<sup>40</sup> The quantities evaluated from adsorption and thermodesorption data provided information about the whole adsorbent-adsorbate system. These data might be used mainly to extract information about porosity of solids,<sup>41</sup> and surface heterogeneity. For instance, the low temperature ( $-196\text{ }^{\circ}\text{C}$ ) nitrogen adsorption is a standard and widely used method to determine the specific surface area and pore size distribution of nanoporous materials.<sup>42</sup>

### Thermogravimetric analysis

Thermogravimetric weight loss curves for MCM-41 and F2 are shown in Figure 2. Pure MCM-41 showed a major weight loss about 7.5% at temperature up to  $105\text{ }^{\circ}\text{C}$ . This could be related to the release of physically surface adsorbed water molecules,<sup>43</sup> which indicated a relatively hydrophobic surface. At higher temperature, TGA curve of MCM-41 was flat, especially up to  $600\text{ }^{\circ}\text{C}$ , showing that there was no remarkable condensation of silanol groups on the surface of the material.<sup>44</sup> In the case of F2, weight loss up to  $100\text{ }^{\circ}\text{C}$  was lower than that of pure MCM-41; indicating the absence of surface adsorbed water molecules due to the presence of surface coverage MLX molecules. At the temperature ranged between  $150$  and  $300\text{ }^{\circ}\text{C}$ , a decrease in weight by about 34% was observed. This could be attributed to the decomposition of MLX pre-loaded, followed by a flat line indicating thermal stability of residual MCM-41.

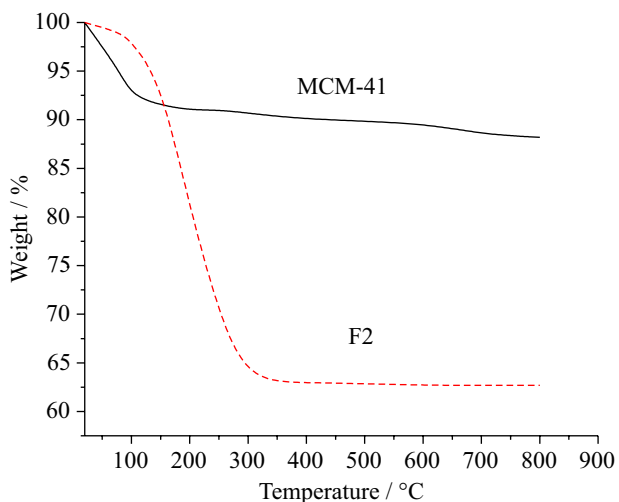


Figure 2. TGA of pure MCM-41 and F2.

### X-ray diffraction analysis

Low-angle XRD patterns of MCM-41, F2 and physical mixture are shown in Figure 3. The XRD of

pure MCM-41 showed a high intensity (100) and two low intensity reflections (110) and (200) at two theta angle corresponding to  $2.51^{\circ}$ ,  $4.49^{\circ}$  and  $5.51^{\circ}$  respectively, which were characteristics of the hexagonal mesoporous MCM-41.<sup>45</sup> For XRD pattern of F2, the (100) and (200) reflections decreased in intensities, which could be due to contrast matching between the silicate framework and MLX organic moieties that were distributed inside the channels of MCM-41. This indicated that there was no observable deformation in the basic structure of MCM-41 with drug loading.<sup>46</sup> XRD pattern of physical mixture showed reflections of MCM-41 indicating the amorphous nature of MLX.

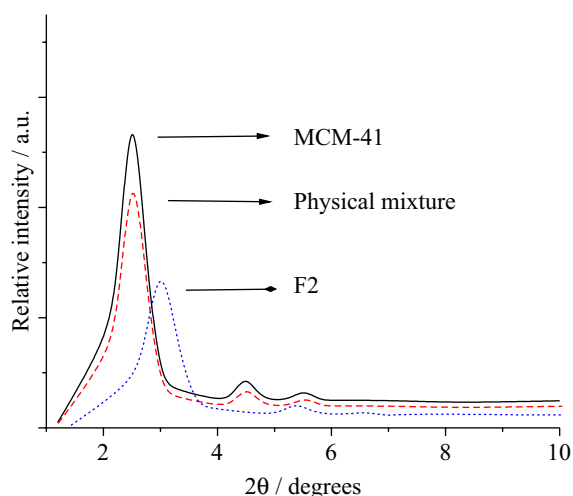
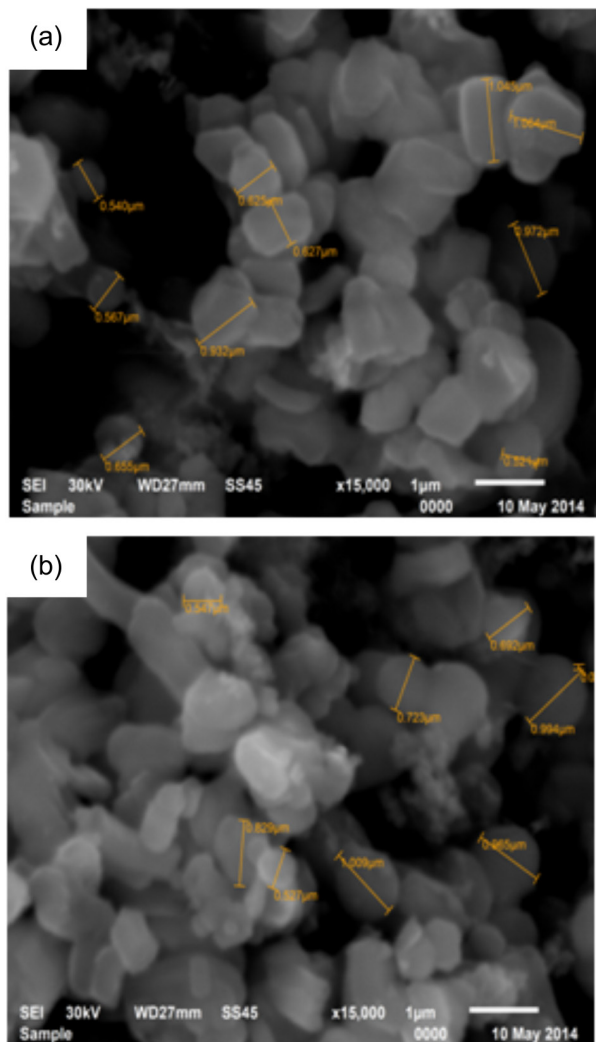


Figure 3. XRD patterns of MCM-41, physical mixture, and F2.

### Morphology and surface area determination

The morphology and particle size of MCM-41 and F2 were analyzed by SEM. The SEM images of MCM-41 and F2 are shown in Figure 4.

The SEM of MCM-41 and F2 showed an irregular particle size ranged between  $0.540$ - $1.064\text{ }\mu\text{m}$  and appeared as fluffy spherical shaped particles. Loading of MLX into MCM-41 did not affect the shape or particle size of MCM-41. This indicated that MLX molecules were entrapped in the pores of MCM-41 particles. Furthermore, the characteristics of MCM-41 and F2 were also confirmed by the results obtained from nitrogen adsorption/desorption measurements (shown in Figure 5), and the detailed data are summarized in Table 1. It was observed that adsorption isotherms, belonged to type-IV as defined by the International Union of Pure and Applied Chemistry (IUPAC) nomenclature, were typical of mesoporous solid.<sup>47</sup> Two samples exhibited a strong adsorption at  $0.4 \geq p/p^{\circ} \geq 0.2$  which, was characteristic to capillary condensation into the uniform pore size mesopores.<sup>48</sup> In addition, it could



**Figure 4.** SEM images of MCM-41 (a) and F2 (b).

be observed that F2 had the similar nitrogen adsorption/desorption isotherm as MCM-41; indicating that the pore dimension of the host material still remained unchanged.<sup>49</sup> The last result was coincided with SEM images and XRD patterns. The data of surface area ( $S_{\text{BET}}$ ,  $\text{m}^2 \text{g}^{-1}$ ), total pore volume ( $V$ ,  $\text{mL g}^{-1}$ ) and average pore radius ( $\bar{r}$ , nm) are summarized in Table 1. Upon inspection of the data shown in Table 1, it could be observed that the  $S_{\text{BET}}$  values and  $V_T$  for F2 decreased than that for MCM-41. This could be related to the corresponding loaded MLX molecules in the pores of MCM-41. The average pore radius decreased from 2.674 to 2.212 nm after MLX loading to prove that MLX molecules were introduced and distributed inside the channel of mesoporous silica.

#### Fourier transform infrared spectroscopy

Infrared spectroscopy has been one of the most frequently used instrumental analysis methods to

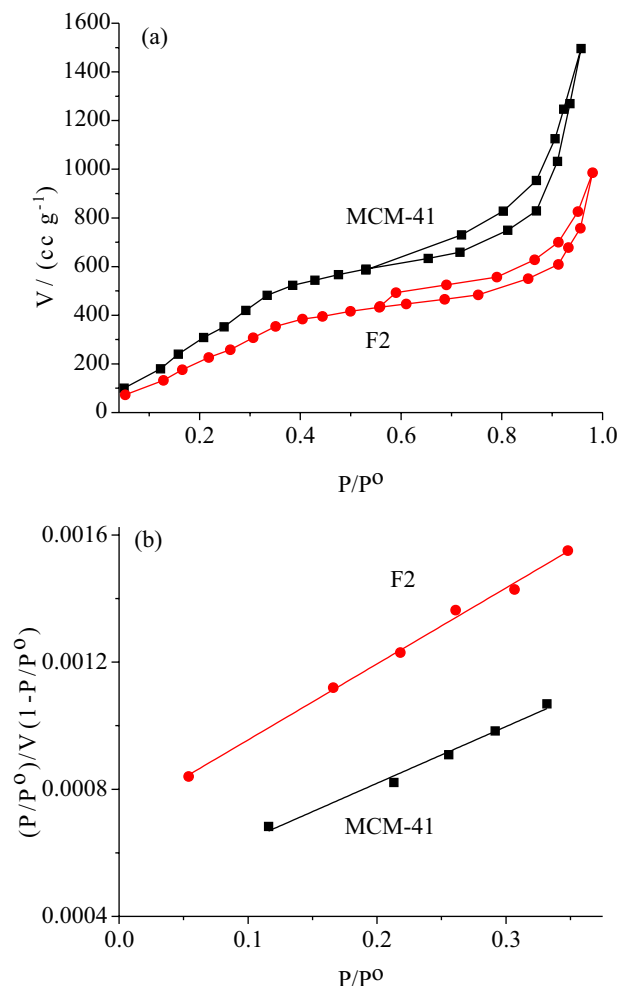


**Figure 5.** Nitrogen adsorption/desorption isotherms (a) and linear BET plot (b) at  $-196^\circ\text{C}$  on MCM-41 and F2.

**Table 1.** Surface area, total pore volume, and average pore radius of MCM-41 and F2

Sample	$S_{\text{BET}} / (\text{m}^2 \text{g}^{-1})$	$V_T / (\text{mL g}^{-1})$	$\bar{r} / \text{nm}$
MCM-41	1640	2.193	2.674
F2	1030	1.139	2.212

characterize the surface functionalities in MCM-41.<sup>48,50</sup> Since its introduction, FTIR spectroscopy has found a wide application to both qualitative and quantitative analysis of the mesoporous silica. The Fourier analysis provides an improvement of the signal-to-noise ratio (S/N), higher energy throughput, greater accuracy of the frequency scale, and the capacity for versatile data manipulation, in competition with dispersive IR spectroscopy. Figure 6 shows FTIR of MCM-41, MLX, physical mixture and F2. With regards to the FTIR spectrum of MCM-41, the presence of a very broad band around  $3480 \text{ cm}^{-1}$  attributed to geminal and associated terminal silanol groups.<sup>51</sup> A broad band at  $1089 \text{ cm}^{-1}$  and a band at  $805 \text{ cm}^{-1}$  related to the

asymmetric and symmetric Si–O stretching vibrations.<sup>52</sup> The bands at 965  $\text{cm}^{-1}$  and 460  $\text{cm}^{-1}$  were corresponding to the stretching and bending vibrations of surface Si–O groups, respectively.<sup>53</sup> The FTIR spectrum of MLX showed its characteristic absorption bands at 3269  $\text{cm}^{-1}$  for O–H or –NH stretching vibrations, 2920  $\text{cm}^{-1}$  for –CONH group, 1620  $\text{cm}^{-1}$  for C=N stretching vibrations, 1535  $\text{cm}^{-1}$  for C–O stretching and 1178  $\text{cm}^{-1}$  for S=O stretching vibration (Figure 6). In the case of the physical mixture, spectrum bands relative to both MCM-41 and MLX were observed indicating the lack of chemical interaction between MLX and MCM-41. The F2 spectrum showed an observable change in bands compared with MCM-41 and MLX (Figure 6); (i) a broad band between 3250  $\text{cm}^{-1}$  and 3260  $\text{cm}^{-1}$  was observed instead of a sharp peak at 3269  $\text{cm}^{-1}$  in case of MLX; (ii) the disappearance of band at 2920  $\text{cm}^{-1}$  which specified for CONH group in case of pure MLX, and (iii) shifting of band 1089  $\text{cm}^{-1}$  belonged to the asymmetric Si–O stretching vibrations in case of pure MCM-41 into 1075  $\text{cm}^{-1}$ . All the last changes suggested that the majority of the MCM-41 isolated terminal silanol groups in F2 interacted with MLX molecules.

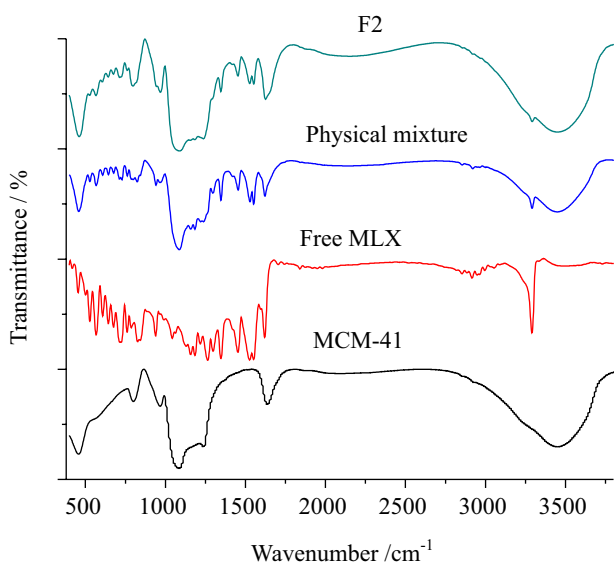


**Figure 6.** FTIR spectra: of MCM-41, MLX, physical mixture, and F2.

#### *In vitro* release studies

The *in vitro* release studies were performed at two pH values: 1.2 and 6.8. These pH values were chosen to observe drug release profile in conditions that mimic the physiological pH of stomach and small intestine. *In vitro* release profiles and release results of MLX- MCM-41 formulations (F1, F2 and F3), free MLX and reference product (R) in 0.1 mol L<sup>-1</sup> HCl (pH 1.2) and phosphate buffer (pH 6.8) are shown and reported in Figure 7 and

Table 2, respectively. MLX solubility was strongly pH-dependent and it displayed low aqueous solubility at acidic pH values below and close to its pKa. The dissolution of all MLX-MCM-41 formulations, free MLX and R product was higher in phosphate buffer (pH 6.8) than in 0.1 mol L<sup>-1</sup> HCl (pH 1.2) (Figure 7 and Table 2). This finding was supported by % drug released at 10 min ( $D_{10\%}$ ) and  $t_{50\%}$  values reported in Table 2. The  $D_{10\%}$  values were ca. 22-37% and ca. 50-63% at pH 1.2 and 6.8, respectively (Table 2). This indicated the increased MLX amount released at pH 6.8. This could be attributed to the weak acidity of MLX (pKa values of 1.1 and 4.2),<sup>54</sup> making it more soluble in alkaline media.

The term “enhanced dissolution” was typically referred to “enhanced release” with mesoporous carriers.<sup>55</sup> Generally, the following four steps take place consecutively after immersing the drug loaded mesoporous materials

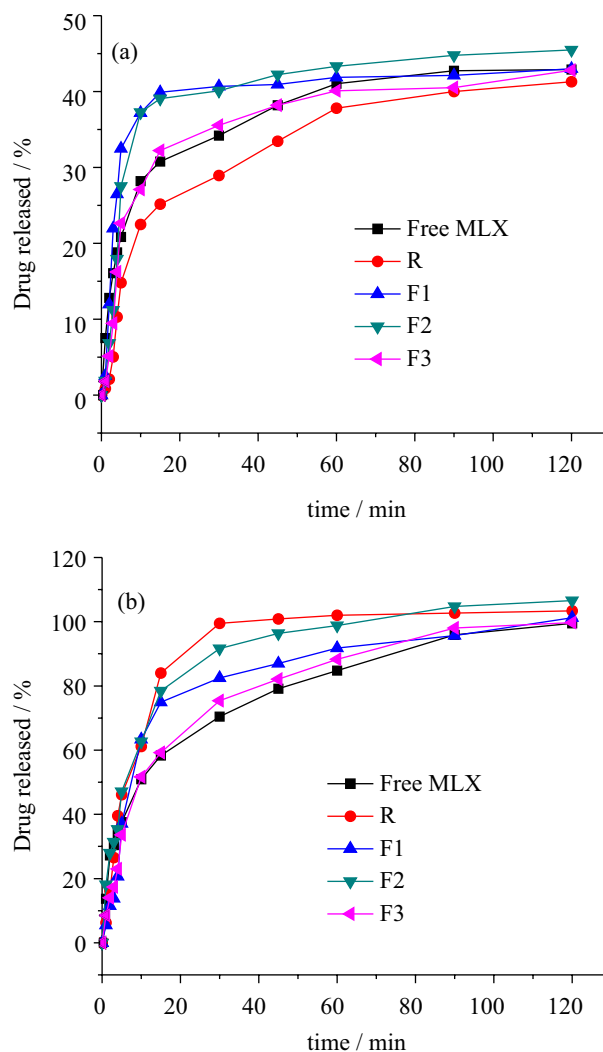


**Figure 7.** Effect of MCM 41 on the dissolution rate of MLX determined by the USP method in (a) 0.1 mol L<sup>-1</sup> HCl (pH 1.2) and (b) phosphate buffer (pH 6.8) at 37 °C.

in biological fluid:<sup>56</sup> (i) absorption of aqueous medium into the mesoporous system driven by capillary forces; (ii) dissolution of drug molecules into the release medium inside the pores; (iii) diffusion of drug molecules out of the mesopores owing to concentration gradients; (iv) diffusion and convectional transport of drug molecules in the release medium.<sup>11</sup> For all MCM-41-MLX formulations (F1, F2 and F3), one might suppose that the increase in the aqueous solubility of MLX at pH 6.8 facilitated the transfer of the molecules from the silica to the buffered solution. In addition to the well-defined porosity with large surface area and channel size of the MCM-41, materials that gave larger possibility of the fluid to penetrate inside the channels and dissolve MLX in the dissolution medium.<sup>56</sup>

The study of drug release kinetics using the zero-order, first-order and Higuchi kinetics was performed (Table 2). By means of the linearization of release profiles the respective correlation coefficients (R) were obtained. The kinetic model which presented higher value of R was considered more appropriate. The release kinetics of all the tested formulations was best fitted to first-order kinetic or Higuchi's model. Although the k values couldn't be used for direct comparison of the profiles, its importance was

related to the half-life of release ( $t_{50\%}$ ) calculation.<sup>57</sup> The  $t_{50\%}$  was of paramount importance because it established the time to promote the dissolution of 50% of the drug. The results indicated differentiated dissolution profiles for the analyzed products in the first 10 min. Therefore, the  $t_{50\%}$  values listed in Table 2, demonstrated a good drug release performance for the tested formulations.

The release profiles of MLX tested formulations in 0.1 mol L<sup>-1</sup> HCl were best fitted to Higuchi's model except F1 and F2 were best fitted to first-order kinetics where the release rate was concentration dependent.<sup>30</sup> Whereas, the release profiles of all MLX tested formulations in phosphate buffer (pH 6.8) were best fitted to first-order kinetics except free MLX was best fitted to Higuchi's model.

Effect of MCM-41 on the dissolution rate of MLX in 0.1 mol L<sup>-1</sup> HCl (pH 1.2) and phosphate buffer (pH 6.8) is shown in Figure 7. This rapid kinetic profile presented a great interest for pharmaceutical application in order to improve a rapid drug delivery of poorly water-soluble drugs. In both dissolution media, all inclusion products had better results than that shown by free MLX (Table 2) whereas, the fastest drug release was obtained from MCM-41-MLX (F1 and F2) (Table 2). Both F1 and F2

**Table 2.** *In vitro* release characteristics, cumulative and differential release parameters of MLX formulations in 0.1 mol L<sup>-1</sup> HCl (pH 1.2) and phosphate buffer (pH 6.8)

Parameter	pH of dissolution medium	Product				
		R	Free MLX	F1	F2	F3
K	1.2	4.39 ± .05	3.80 ± .04	0.050 ± 0.001	0.06 ± 0.01	6.5 ± 0.2
	6.8	0.09 ± 0.002	7.9 ± 0.06	0.11 ± 0.003	0.123 ± 0.066	0.072 ± 0.001
$t_{50\%}$ / min	1.2	63.4 ± 0.07	71.70 ± .08	11.3 ± 2.3 <sup>a</sup>	12.8 ± 0.38 <sup>a</sup>	29.7 ± 0.6 <sup>a</sup>
	6.8	7.12 ± 0.04	15.6 ± 2.1	6.17 ± 0.18 <sup>a</sup>	6.59 ± 3.57 <sup>a</sup>	9.5 ± 0.21 <sup>a</sup>
Order	1.2	Higuchi	Higuchi	First	First	Higuchi
	6.8	First	Higuchi	First	First	First
D <sub>10</sub> / %	1.2	22.5 ± 2.1	20.2 ± 3.5	37.1 ± 2.3 <sup>a</sup>	37.2 ± 4.1 <sup>a</sup>	27.0 ± 2.9
	6.8	61.1 ± 4.1	50.9 ± 5.1	63.3 ± 2.2	62.6 ± 4.3	51.6 ± 3.2
D <sub>120</sub> / %	1.2	41.2 ± 1.5	42.9 ± 1.2	42.9 ± 2.1	45.4 ± 2.2	42.8 ± 1.4
	6.8	99.4 ± 2.3	103.4 ± 2.1	101.2 ± 3.4	106.5 ± 4.1	99.6 ± 3.4
AUCC / min%	1.2	4731.9 ± 399.1	4500.8 ± 197.1	4828.2 ± 21.0	4932.6 ± 192.0	4424.2 ± 205.0
	6.8	11306.2 ± 156.1	9576.4 ± 976.0	10224.6 ± 130.7	11136.3 ± 509.4	9799.3 ± 42.2
PH / (% released)	1.2	7.7 ± 0.9	7.5 ± 1.2	13.8 ± 0.2 <sup>a</sup>	14.5 ± 1.4 <sup>a</sup>	7.09 ± 1.3
	6.8	22.9 ± 1.2	13.6 ± 0.9	22.9 ± 5.1	26.2 ± 0.2	18.0 ± 3.4
PT / min	1.2	3.0 ± 0.0	3.0 ± 0.0	2.6 ± 0.5 <sup>a</sup>	2.3 ± 0.5 <sup>a</sup>	2.6 ± 0.5
	6.8	3.0 ± 0.0	3.0 ± 0.0	2.6 ± 0.5 <sup>a</sup>	2.0 ± 0.0 <sup>a</sup>	2.6 ± 0.5
AUDC / min%	1.2	396.7 ± 19.9	316.3 ± 28.2	239.5 ± 35.6 <sup>a</sup>	147.5 ± 45.7 <sup>a</sup>	288.4 ± 11.7
	6.8	672.5 ± 45.6	1011.5 ± 105.4	834.5 ± 44.7 <sup>a</sup>	805.4 ± 22.9 <sup>a</sup>	1020.2 ± 64.1

<sup>a</sup>Significantly different from R at  $p < 0.05$ . Values are presented as the arithmetic mean (SD); n = 3. K: release rate constant;  $t_{50\%}$ : half life; D<sub>10</sub>: % drug dissolved at 10 min; D<sub>120</sub>: % drug dissolved at 120 min; AUCC: area under cumulative curve; PH: peak height; PT: peak time; and AUDC: area under differential curve. Units for K are (mg min<sup>-1/2</sup>) for Higuchi and (min<sup>-1</sup>) for first order.

formulations provided the best MLX release and were best fitted to first-order kinetics in both dissolution media (Table 2). The dissolution profile similarity was calculated using a statistical similarity factor  $f_2$ , as defined in the international guidelines.<sup>58</sup> Comparison between F1 with F2 formulations suggested that F2 dissolution did not match F1. The results indicated that the values of the similarity factor  $f_2$  were 45.3% and 21.7% (< 50%) in 0.1 mol L<sup>-1</sup> HCl (pH 1.2) and phosphate buffer (pH 6.8), respectively, signifying difference between the compared formulations. F2 showed the highest PH values (% released) and the lowest PT (min) values in both dissolution media. The PH values of F2 were 14.5% and 26.2% in pH 1.2 and 6.8, respectively (Table 1). The PT values were 2.3 and 2.0 min in pH 1.2 and 6.8, respectively (Table 2). Accordingly, F2 was selected for the *in vivo* study.

#### Physical stability studies

Humidity and temperature are two important factors responsible for product physical instability during normal storage conditions. Both of them may promote the organization of adsorbed MLX molecules in crystals.<sup>16</sup> As such, the drug dissolution profiles might be modified in respect to the starting product with a consequent change in final drug bioavailability. For this reason, it was important to evaluate F2 stability both in presence of CaCl<sub>2</sub> at room temperature and at high humidity (75%) in stressed temperature conditions (40 °C). The physical stability, monitored by XRD, was conducted at predetermined intervals. XRD diffractograms demonstrated that F2 maintained its physical characteristics and no crystals formation was detected during the experimental procedure. This was probably due to occurrence of interactions between MCM-41 silanols and the drug molecules which stabilized the system, and to the fact that drug molecules are stored in a nanosized space preventing from re-crystallization.<sup>17</sup>

#### *In vivo* study

The therapeutic efficacy of MLX is strongly limited by its poor water solubility (0.012 mg mL<sup>-1</sup>).<sup>21</sup> Apart from low aqueous solubility, MLX also has a high degree of enterohepatic circulation and long half-life.<sup>59</sup> Thus, a formulation which permits a fast MLX release in its absorption window could be very useful. In order to achieve this aim, mesoporous MCM-41 was chosen as carrier to improve MLX dissolution rate in gastric conditions and consequently a better drug absorption. From the results of the preceding *in vitro* study, F2 and free MLX without any additives were selected for the *in vivo* study. Also, the

marketed product of MLX (Mobic®) was considered for the *in vivo* study as R product.

The non-compartmental PK parameters were calculated (Table 2) from the plasma concentration-time curve of each rabbit after administration of an oral dose of MLX (5 mg kg<sup>-1</sup>) from the three products (R, free MLX and F2). The average plasma concentration-time curves are shown in Figure 8. Moderate intersubject variability was encountered in plasma MLX concentrations as previously reported in rabbits.<sup>60</sup> The results of this study were in a good agreement with the results of the other studies of MLX in rabbits; elimination rate constants, and half-lives, compared quite closely,<sup>60-62</sup> which emphasizes the validity of the present results.

Administration of free MLX to rabbits resulted in an AUC<sub>0-∞</sub> value of 11.9 μg h mL<sup>-1</sup> and a T<sub>max</sub> of 4.3 h. When the same dose of MLX was introduced as R or formulated into MCM-41 (F2), the systemic exposure to MLX was raised significantly by ca. 4-fold as reflected in AUC<sub>0-∞</sub> values of 46.9 and 45.5 μg h mL<sup>-1</sup> for R and F2, respectively. In addition, T<sub>max</sub> decreased to 3.9 h in case of F2.

It has been shown that MLX presented a two distinct double-peak profile after oral administration in case of R and F2. However, in case of rabbits receiving free MLX, their plasma profiles showed nearly a plateau in the time interval corresponding to the second peak. The first average plasma concentration peak (C<sub>max1</sub>) values were 6.1, 0.91 and 5.8 μg mL<sup>-1</sup> observed at 4.3, 4.3 and 3.9 h (T<sub>max1</sub>) for R, free MLX and F2, respectively. The second average peak (C<sub>max2</sub>) values were 5.4 and 5.0 μg mL<sup>-1</sup> observed at 6.6-6.5 h (T<sub>max2</sub>) for R and F2, respectively. These two distinct peaks could be due to the rapid release of MLX in case of F2 and R in comparison with free MLX. This was confirmed by the *in vitro* release results that indicated high initial release of MLX from F2 and R products compared with free MLX in both dissolution media (Table 2). Thus, F2 and R gave early high presentation of MLX to the main absorption site of drug absorption (the upper part of the small intestine), which could be responsible for the first peak in the plasma profiles of F2 and R compared with free MLX. The second peak was due to the subsequently released drug after bypassing the main absorption site and the enterohepatic cycling.<sup>63,64</sup> As such, the second peak was of lower intensity compared with the first peak (Table 3). C<sub>max</sub>, peak plasma concentration; t<sub>max</sub>, time to reach peak plasma concentration; AUC<sub>0-∞</sub>, area under the concentration-time curve from zero to infinity; AUC<sub>0-t</sub>, area under the concentration-time curve from zero to the last measurable plasma concentration; AUC<sub>t-∞</sub>, area under the concentration-time curve from the last measurable concentration to infinity; t<sub>1/2</sub>, elimination half-life; MRT,

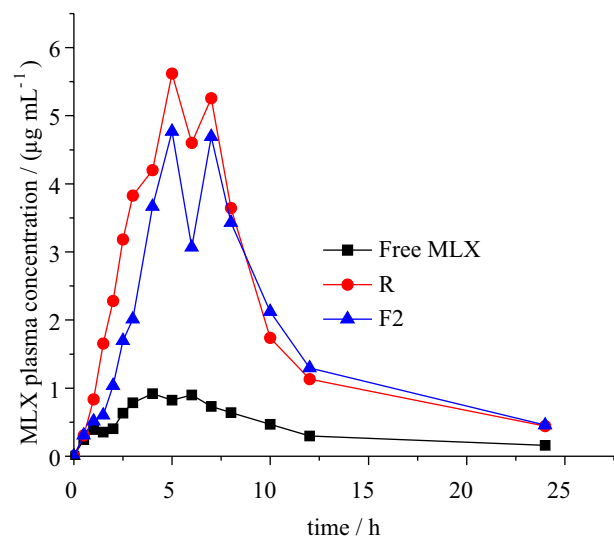


**Figure 8.** Mean MLX plasma concentration-time profiles after a single oral administration of free MLX, reference product (Mobic® BoehringerIngelheim International GmbH Ingelheim am Rhein, Germany) and MCM-41 loaded with MLX in rabbits (n = 5).

**Table 3.** Pharmacokinetic parameters of MLX after a single oral dose administration to 6 healthy male rabbits

Parameter	R	Free MLX	F2
$C_{max1}$ / ( $\mu\text{g mL}^{-1}$ )	$6.1 \pm 1.2$	$0.91 \pm 0.3$	$5.8 \pm 1.4$
$C_{max2}$ / ( $\mu\text{g mL}^{-1}$ )	$5.4 \pm 0.8$	–	$5.0 \pm 1.6$
$T_{max1}$ / h	$4.3 \pm 1.1$	$4.3 \pm 0.6$	$3.9 \pm 0.5^a$
$T_{max2}$ / h	$6.6 \pm 0.5$	–	$6.5 \pm 0.6$
$AUC_{0-t}$ / ( $\mu\text{g h mL}^{-1}$ )	$42.0 \pm 4.1$	$9.9 \pm 1.8^b$	$41.2 \pm 4.2$
$AUC_{0-\infty}$ / ( $\mu\text{g h mL}^{-1}$ )	$46.9 \pm 3.4$	$11.9 \pm 1.7^b$	$45.5 \pm 5.3$
$t_{1/2}$ / h	$7.6 \pm 0.5$	$8.7 \pm 2.6$	$6.9 \pm 0.6$
MRT	$7.5 \pm 0.7$	$7.7 \pm 1.6$	$6.8 \pm 1.3^a$
Cl/F / ( $\text{L h}^{-1}$ )	$0.32 \pm 0.04$	$1.26 \pm 0.2$	$0.32 \pm 0.08$
Vd/F / L	$2.4 \pm 0.4$	$9.76 \pm 2.4$	$2.6 \pm 0.7$

Values are presented as the arithmetic mean (SD). <sup>a</sup>Significantly different from R at  $p < 0.05$ ; <sup>b</sup>significantly different from F2 and R at  $p < 0.05$ .

mean residence time clearance; and  $V_d/F$ , volume of distribution.

The GI absorption of MLX is dissolution rate limited (BCS class II). Thus the rate of drug absorption (represented by  $T_{max}$ ) from the tested products (R, free MLX and F2) reflected mainly the rate of drug dissolution (represented by  $t_{50\%}$ ), which depended mainly on the formulation characteristics of the tested products. F2 showed the smallest rate of drug absorption (3.9 h) in comparison with R (4.3 h) (Table 3). In addition to the smallest MRT value (6.8 h) in comparison with R (7.5 h). These PK profiles of MLX in rabbits reflected the *in vitro* dissolution enhancement achieved when MCM-41 is used as a carrier for MLX. These findings were correlated with the *in vitro*

results where the highest dissolution rate was achieved with F2 in comparison with R in the two dissolution media (Table 2). Concerning the extent of MLX absorption, the plasma levels of MLX obtained after oral dosing of F2 were similar to those obtained from R (Figure 8). Both R and F2 showed a comparable higher AUC compared with free MLX (Table 3). This finding was coincided with the results of AUCC from the *in vitro* results (Table 2). Accordingly, that the effect of MCM-41 was mainly on the rate not the extent of MLX absorption. This might be attributed to the effect of MCM-41 on the rate of drug dissolution. These results indicated the suitability of formulation procedure for preparation of MCM-41- MLX with significantly improved *in vitro* dissolution rate, and enhanced fast onset of therapeutic drug effect.

## Conclusions

MCM-41 is a promising carrier to enhance the dissolution of poorly water soluble compounds such as MLX. In the present study, the biopharmaceutical performance of mesoporous silica material (MCM-41) as a carrier for the poorly water soluble drug MLX was investigated. MLX solubility was strongly pH-dependent and it displayed low aqueous solubility at acidic pH values below and close to its pKa. The effect of MCM-41 was mainly on the rate not the extent of MLX absorption. These results evidence that ordered mesoporous silica is a promising carrier to achieve enhanced oral bioavailability for drugs with extremely low water solubility.

## Supplementary Information

Supplementary data (TGA, FTIR spectra, XRD, SEM, nitrogen adsorption/desorption isotherms and linear BET plots for F1 and F3 samples) are available free of charge at <http://jbcs.sbq.org.br> as PDF file.

## Acknowledgment

The authors acknowledge the research sector of Damanshour University for financial support. Authors would like to thank the editors of Journal of Brazilian Chemical Society and referees for their many instructive comments, which greatly improved the original version.

## References

1. Varma, M. V.; Khandavilli, S.; Ashokraj, Y.; Jain, A.; Dhanikula, A.; Sood, A.; Pillai, N. S.; Sharma, P.; Gandhi, A. S.; Nair, V.; Panchagnula, R.; *Curr. Drug Metab.* **2004**, *5*, 375.

2. Lipinski, C.; *Am. Pharm. Rev.* **2002**, *5*, 582.
3. Amidon, G. L.; Lennernäs, H.; Shah, V. P.; Crison, J. R.; *Pharm. Res.* **1995**, *12*, 413.
4. Zhang, P.; Forsgren, J.; Strømme, M.; *Int. J. Pharm.* **2014**, *472*, 185.
5. Beck, J. S.; Vartuli, J. C.; Oth, W.; Leonowicz, M. E.; Kresge, C. T.; Schmitt, K. D.; Chu, C. J. W.; Olson, D. H.; Sheppard, E. W.; McCullen, S. B.; Huggins, J. B.; Schlenker, I. L.; *J. Am. Chem. Soc.* **1992**, *114*, 10834.
6. Lee, J. W.; Cho, D. I.; Shim, W. G.; Moo, H.; *Korean J. Chem. Eng.* **2004**, *21*, 246.
7. Melero, J. A.; Grieken, R. V.; Morales, G.; *Chem. Rev.* **2006**, *106*, 3790.
8. Ambroggi, V.; Perioli, L.; Marmottini, F.; Giovagnoli, S.; Esposito, M.; Rossi, C.; *Eur. J. Pharm. Sci.* **2007**, *32*, 216.
9. Jessy, S.; Dhanila, V.; *Int. J. Pharm. Invest.* **2013**, *43*, 405.
10. Salonen, J.; Kaukonen, A. M.; Hirvonen, J.; Lehto, V. P.; *J. Pharm. Sci.* **2008**, *97*, 632.
11. Sameer, S.; Praveen, S.; Shraddha, B.; Atmaram, P. P.; *AAPS PharmSciTech* **2005**, *6*, 618.
12. Thomas, M. J.; Slipper, I.; Walunj, A.; Jain, A.; Favretto, M. E.; Kallinteri, P.; Douroumis, D.; *Int. J. Pharm.* **2010**, *387*, 272.
13. Tingming, F.; Liwei, G.; Kang, L.; Tianyao, W.; Jin, L.; *Appl. Surf. Sci.* **2010**, *256*, 6963.
14. Ciesla, U.; Schüth, F.; *Microporous Mesoporous Mater.* **1999**, *27*, 131.
15. Brühwiler, D.; Calzaferri, G.; *Microporous Mesoporous Mater.* **2004**, *72*, 1.
16. Ambroggi, V.; Perioli, L.; Pagano, C.; Latterini, L.; Marmottini, F.; Ricci, M.; Rossi, C.; *Microporous Mesoporous Mater.* **2012**, *147*, 343.
17. Sliwinska-Bartkowiak, M.; Dudziak, G.; Gras, R.; Sikorski, R.; Radhakrishnan, R.; Gubbins, K. E.; *Colloids Surf., A* **2001**, *187*, 523.
18. Engelhardt, G.; Homma, D.; Schlegel, K.; Utmann, R.; Schnitzler, C.; *Inflammation Res.* **1995**, *44*, 423.
19. Ambrus, R.; Kocbek, P.; Kristl, J.; Sibanc, R.; Rajkó, R.; Szabó-Révész, P.; *Int. J. Pharm.* **2009**, *381*, 153.
20. Farid, M.; El-Setouhy, D. A.; El-Nabarawi, M. A.; El-Bayomi, T.; *J. Drug Del. Sci. Tech.* **2014**, *24*, 645.
21. Seedher, N.; Bhatia, S.; *AAPS PharmSciTech* **2003**, *4*, 36.
22. Türeck, D. I.; Busch, U.; Heinzl, G.; Nar, H.; *Arzneim. Forsch.* **1997**, *47*, 253.
23. Davies, N. M.; Skjold, N. M.; *Clin. Pharmacokinet.* **1999**, *36*, 115.
24. Helmy, S. A.; El Bedaiwy, H. M.; *Drug Res.* **2013**, *63*, 331.
25. Heikkilä, T.; Salonen, J.; Tuura, J.; Kumar, N.; Salmi, T.; Murzin, D. Y.; Hamdy, M. S.; Mul, G.; Laitinen, L.; Kaukonen, A. M.; Hirvonen, J.; Lehto, V. P.; *Int. J. Pharm.* **2007**, *14*, 337.
26. Ramila, P. H. A.; Perez-Pariente, J.; Vallet-Regi, M.; *Microporous Mesoporous Mater.* **2004**, *68*, 105.
27. Al-Kady, A. S.; Gaber, M.; Hussein, M. M.; Ebeid, El-Z. M.; *Eur. J. Pharm. Biopharm.* **2011**, *77*, 66.
28. Hu, Y.; Zhi, Z.; Zhao, Q.; Wu, C.; Zhao, P.; Jiang, H.; Jiang, T.; Wang, S.; *Microporous Mesoporous Mater.* **2012**, *147*, 94.
29. Halamová, D.; Zelenák, V.; *J. Inclusion Phenom. Macrocyclic Chem.* **2012**, *72*, 15.
30. Beck, J. S.; Vartuli, J. C.; Roth, W. J.; Leonowics, M. E.; Kresge, C. T.; Schmitt, K. D.; Chu, C. T. W.; Olson, D. H.; Sheppard, E. W.; McCullen, S. B.; Higgins, J. B.; Schlenker, J. L.; *J. Am. Chem. Soc.* **1992**, *114*, 10834.
31. Bourne, D. W.; Banker, G. S.; Rhodes, C. T.; *Modern Pharmaceuticals*, Marcel Dekker Inc: New York, 2002.
32. EL-Yazigi, A.; *J. Pharm. Sci.* **1998**, *70*, 535.
33. Nikolic, L.; Djuric, Z.; Jovanovic, M.; *J. Pharm. Sci.* **1992**, *81*, 386.
34. Higuchi, T.; *J. Pharm. Sci.* **1963**, *52*, 1145.
35. <http://grants.nih.gov/grants/olaw/guidebook.pdf> accessed in May, 2014.
36. <http://www.fda.gov/downloads/Drugs/Guidances/ucm070107.pdf> accessed in May, 2014.
37. Hedaya, M. A.; *Basic Pharmacokinetics*, Taylor and Francis: Boca Raton, Florida, USA, 2007.
38. Pinnavaia, T. J.; Thorpe, M. F.; *Access in Nanoporous Materials*, Plenum Press: New York, 1995.
39. Rudzinski, W.; Everett, D. H.; Gregg, S. J.; Sing, K. S. W.; *Adsorption, Surface Area and Porosity*, Academic Press: London, 1991.
40. Wunderlich, B.; *Thermal Analysis*, Academic Press: New York, 1990.
41. Kruk, M.; Jaroniec, M.; Sayari, A.; *Adsorption* **2000**, *6*, 47.
42. Bandosz, J. T.; *Activated Carbon Surfaces in Environmental Remediation*, The City College of New York: New York, 2006.
43. Jaroniec, C. P.; Gilpin, R. K.; Jaroniec, J.; *J. Phys. Chem. B* **1979**, *101*, 6861.
44. Uysal, B.; *J. Chem. Sci.* **2013**, *125*, 1385.
45. Park, S. E.; Kim, D. S.; Chang, J. S.; Kim, W. Y.; *Catal. Today* **1998**, *44*, 301.
46. Zhao, H.; Zho, L.; Cai, M.; *React. Kinet., Mech. Catal.* **2010**, *100*, 187.
47. Brunauer, S.; Deming, L. S.; Deming, W. S.; Teller, E.; *J. Am. Chem. Soc.* **1940**, *62*, 1723.
48. Kong, Y.; Jiang, S. Y.; Wang, J.; Wang, S. S.; Yan, Q.; Lu, Y.; *Microporous Mesoporous Mater.* **2005**, *86*, 191.
49. Qua, F.; Zhua, G.; Lina, H.; Zhanga, H.; Suna, J.; Lia, S.; Qiu, S.; *J. Solid State Chem.* **2006**, *179*, 2027.
50. Nastase, S.; Bajenaru, L.; Matei, C.; Mitran, R. A.; Berger, D.; *Microporous Mesoporous Mater.* **2013**, *182*, 32.
51. Ambroggi, V.; Perioli, L.; Pagano, C.; Latterini, L.; Marmottini, F.; Ricci, M.; Rossi, C.; *Microporous Mesoporous Mater.* **2012**, *147*, 343.

52. Romero, A. A.; Alba, M. D.; Zhou, W.; Klinowski, J.; *J. Phys. Chem. B* **1997**, *101*, 5294.
53. Takahashi, R.; Sato, S.; Sodesawa, T.; Kawakita, M.; Ogura, K.; *J. Phys. Chem. B* **2000**, *104*, 12184.
54. Peter, L.; Klaus, D.; Wolfhard, E.; Günter, T.; Klaus, W.; *Eur. J. Pharm. Sci.* **1996**, *4*, 175.
55. Xu, W.; Riikonen, J.; Lehto, V. P.; *Int. J. Pharm.* **2013**, *453*, 181.
56. Charnay, C.; Bégu, S.; Tourné-Péteilh, C.; Nicole, L.; Lerner, D. A.; Devoisselle, J. M.; *Eur. J. Pharm. Biopharm.* **2004**, *57*, 533.
57. Oliveira, É.; Azevedo, R.; Bonfilio, R.; Oliveira, D.; Ribeiro, G.; Araújo, M. D.; *Braz. J. Pharm. Sci.* **2009**, *45*, 67.
58. <http://www.fda.gov/downloads/Drugs/GuidanceComplianceRegulatory-Information/Guidances/ucm070124.pdf> accessed in January, 2014.
59. Davies, N. M.; Skojdt, N. M.; *Clin. Pharmacokinet.* **1999**, *36*, 115.
60. Turner, P. V.; Chen, H. C.; Taylor, W. M.; *Comp. Med.* **2006**, *56*, 63.
61. Fredholm, D. V.; Carpenter, J. W.; KuKanich, B.; Kohles, M.; *Am. J. Vet. Res.* **2013**, *74*, 636.
62. Carpenter, J. W.; Pollock, C. G.; Koch, D. E.; Hunter, R. P.; *J. Zoo Wildlife Med.* **2009**, *40*, 601.
63. Busch, U.; Heinzl, G.; Narjes, H.; *Eur. J. Clin. Pharmacol.* **1995**, *48*, 269.
64. Lehr, T.; Staab, A.; Tillmann, C.; Trommeshauser, D.; Schaefer, H. G.; Kloft, C.; *Clin. Pharmacokinet.* **2009**, *48*, 529.

Submitted: January 29, 2015

Published online: April 30, 2015